



# HHS Public Access

Author manuscript

Cell Rep. Author manuscript; available in PMC 2020 April 10.

Published in final edited form as:

Cell Rep. 2020 March 17; 30(11): 3691–3698.e5. doi:10.1016/j.celrep.2020.02.084.

## Differential Modes of Orphan Subunit Recognition for the WRB/CAML Complex

Alison J. Inglis<sup>1</sup>, Katharine R. Page<sup>1</sup>, Alina Guna<sup>1,2</sup>, Rebecca M. Voorhees<sup>1,3,\*</sup>

<sup>1</sup>Division of Biology and Biological Engineering, California Institute of Technology, Pasadena, CA 91125, USA

<sup>2</sup>Present address: Department of Cellular and Molecular Pharmacology, University of California, San Francisco, CA 94158, USA

<sup>3</sup>Lead Contact

### SUMMARY

A large proportion of membrane proteins must be assembled into oligomeric complexes for function. How this process occurs is poorly understood, but it is clear that complex assembly must be tightly regulated to avoid accumulation of orphan subunits with potential cytotoxic effects. We interrogated assembly in mammalian cells by using the WRB/CAML complex, an essential insertase for tail-anchored proteins in the endoplasmic reticulum (ER), as a model system. Our data suggest that the stability of each subunit is differentially regulated. In WRB's absence, CAML folds incorrectly, causing aberrant exposure of a hydrophobic transmembrane domain to the ER lumen. When present, WRB can correct the topology of CAML both *in vitro* and in cells. In contrast, WRB can independently fold correctly but is still degraded in the absence of CAML. We therefore propose that there are at least two distinct regulatory pathways for the surveillance of orphan subunits in the mammalian ER.

### In Brief

Most membrane proteins assemble into multi-subunit complexes. How unassembled subunits are recognized and triaged for degradation is poorly understood. Inglis et al. use the WRB/CAML complex to define two modes of orphan recognition: CAML folds incorrectly without WRB, exposing a degron, while WRB inserts correctly but is degraded when unassembled.

### Graphical Abstract

---

This is an open access article under the CC BY-NC-ND license (<http://creativecommons.org/licenses/by-nc-nd/4.0/>).

\*Correspondence: [voorhees@caltech.edu](mailto:voorhees@caltech.edu).

#### AUTHOR CONTRIBUTIONS

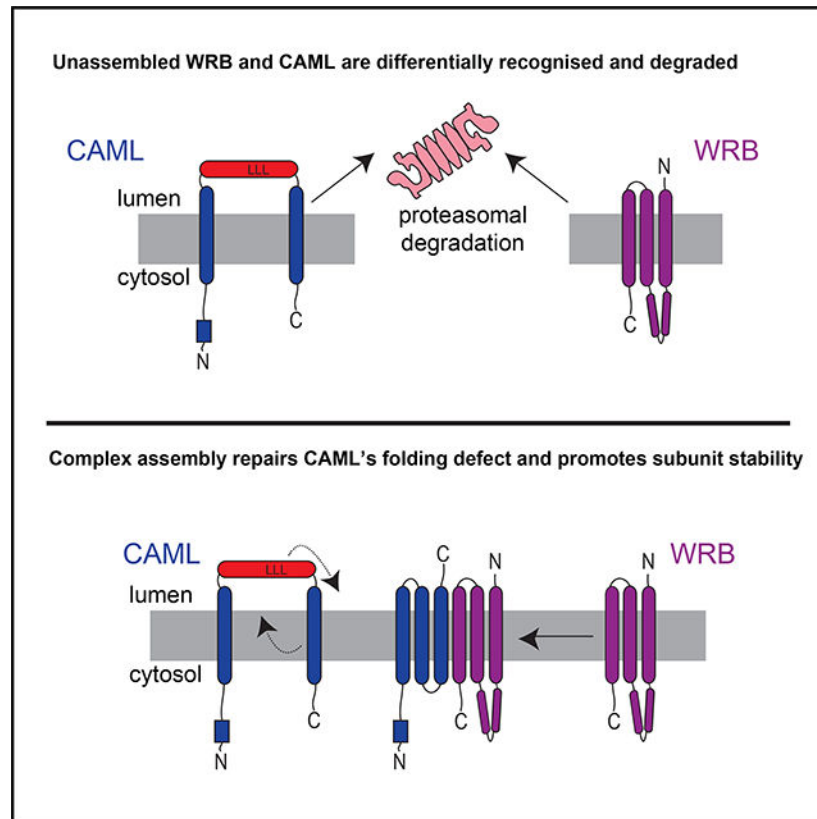
A.J.I., A.G., and R.M.V. conceived and designed the study. A.J.I., K.R.P., and A.G. performed the experiments. R.M.V. wrote the manuscript with input from all authors.

#### DECLARATION OF INTERESTS

The authors declare no conflict of interest.

#### SUPPLEMENTAL INFORMATION

Supplemental Information can be found online at <https://doi.org/10.1016/j.celrep.2020.02.084>.



## INTRODUCTION

A large fraction of the proteome is organized into multi-subunit complexes that must be assembled at a defined stoichiometry (Huttlin et al., 2017; Marsh and Teichmann, 2015). In the cytosol, unassembled subunits expose thermodynamically unfavorable interfaces to the crowded cellular environment, which could lead to aggregation and cytotoxic effects (Sung et al., 2016; Yanagitani et al., 2017). As a result, assembly of these complexes is tightly regulated to ensure that orphan subunits, which have been synthesized in excess or cannot be assembled, are rapidly degraded to maintain cellular homeostasis (Harper and Bennett, 2016; Shemorry et al., 2013; Sung et al., 2016; Xu et al., 2016; Yanagitani et al., 2017). Despite increasing interest in cytosolic complex assembly, how multi-subunit membrane protein assembly is regulated remains poorly understood (Dephoure et al., 2014).

Most membrane proteins are synthesized at the ER where their hydrophobic transmembrane domains (TMDs) must be inserted into the lipid bilayer, most commonly by the Sec61 insertion channel (Rapoport, 2007). A large proportion of membrane proteins must be further assembled into oligomeric complexes for function. Several lines of evidence suggest that this assembly process is highly regulated within the ER. First, orphan subunits of oligomeric membrane protein complexes are unstable and rapidly degraded by the ubiquitin-proteasome pathway (Juszkiewicz and Hegde, 2018; Lippincott-Schwartz et al., 1988). Second, many membrane protein subunits require charged or polar residues for function or oligomerization, which prior to assembly would be exposed and, thereby, disfavored in the

lipid bilayer. Finally, many TMDs situated at subunit interfaces are suboptimal and not predicted to insert autonomously, raising the question of how their insertion is coordinated with subunit assembly. Therefore, the mechanisms regulating oligomeric assembly within the ER are likely to be as defined and stringent as those in the cytosol.

Recent work demonstrates that in the cytosol, many multi-subunit complexes assemble co-translationally (Shiber et al., 2018): interaction between subunits occurs upon emergence of nascent domains from the ribosome, resulting in the temporal integration of polypeptide folding and oligomeric assembly. However, unlike in the cytosol, the steric constraints of the two-dimensional lipid bilayer, combined with the fact that the Sec61 channel is surrounded by over 20 integral membrane proteins, severely limits the space available for simultaneous insertion and oligomerization. How membrane proteins overcome these additional challenges to coordinate the folding and assembly of multiprotein complexes within the ER remains unknown.

To better understand membrane protein assembly and quality control in the mammalian ER, we have chosen to study the regulation of the WRB/CAML complex. WRB (tryptophan-rich basic protein) and CAML (calcium-modulating cyclophilin ligand [Get1/2 in yeast]) together form an insertase for tail-anchored proteins (Vilardi et al., 2011, 2014; Yamamoto and Sakisaka, 2012). Previous work suggests that WRB and CAML stability is interdependent, consistent with it assembling into an obligate oligomeric complex (Colombo et al., 2016; Rivera-Monroy et al., 2016). The interaction between the two subunits is thought to be mediated by the TMDs, suggesting that a TMD-mediated degron may be exposed in the absence of the subunits' cognate binding partner (Vilardi et al., 2014; Wang et al., 2014; Yamamoto and Sakisaka, 2012). Despite this, the stoichiometry of the WRB/CAML complex remains to be precisely determined, as earlier work suggests CAML is in 5-fold excess of WRB *in vivo*; however, no isolated populations of CAML or WRB were detected by blue native-PAGE analysis of mammalian cells, suggesting CAML and WRB are always found in stable oligomeric complexes (Carvalho et al., 2019; Colombo et al., 2016).

Here, we report data suggesting at least two distinct mechanisms for the regulation of orphan membrane protein subunits, as exemplified by the WRB/CAML complex: (1) WRB is representative of a larger class of membrane subunits that insert independently but remain subject to degradation in the absence of their binding partners; and (2) in contrast, CAML inserts incorrectly in the absence of WRB, aberrantly exposing a hydrophobic TMD to the ER lumen, which acts as a flag for degradation. Upon co-expression with WRB, we observe a topological change to CAML, suggesting that WRB acts as a chaperone for folding and assembly of the WRB/CAML complex. These observations set the stage for future work studying the regulation of the diversity of membrane protein subunits that must assemble at the ER.

## RESULTS AND DISCUSSION

### WRB and CAML Are Destabilized in the Absence of Their Binding Partner

Earlier work has established that WRB and CAML expression is interdependent, although previous reports suggest that this regulation may occur partially at the transcriptional level (Carvalho et al., 2019; Colombo et al., 2016; Rivera-Monroy et al., 2016; Shing et al., 2017). We reasoned that there may be an additional layer of regulation of WRB and CAML at the post-translational level, as has been observed for other multi-subunit complexes (Béguin et al., 1998; Bonifacino et al., 1990, 1991; Dephoure et al., 2014; Lippincott-Schwartz et al., 1988; Minami et al., 1987; Volkmar et al., 2019). To measure WRB and CAML stability, we used a fluorescent reporter system in which a single open reading frame encodes a green fluorescent protein (GFP) fusion of WRB or CAML, followed by a red fluorescent protein (RFP), separated by a viral 2A sequence (Figure 1A). We first demonstrated that the introduction of these fluorescent tags does not affect WRB and CAML association in HEK293T cells (Figure S1A). Therefore, ratio-metric analysis of GFP:RFP fluorescence using flow cytometry can be used as a proxy for subunit stability at the protein level (Itakura et al., 2016).

Exogenous expression of either WRB or CAML individually results in the rapid degradation of excess subunits, suggesting that each protein is independently unstable (approximately 65% of overexpressed WRB and 80% of overexpressed CAML that is synthesized is degraded; Figure S1B). We observe a further decrease in the levels of both WRB and CAML upon small interfering RNA (siRNA) knockdown of their endogenous binding partner, indicating that orphaned WRB and CAML are destabilized (Figure 1A). Consistent with tight regulation of CAML and WRB levels by the cellular quality control machinery, we observe that overexpression of either subunit results in downregulation of the endogenous protein and upregulation of its binding partner, as has been observed for other obligate hetero-oligomeric complexes (Figure S1C; Guna et al., 2018; Juskiewicz and Hegde, 2017).

### Two Distinct Mechanisms for Recognition of Orphan Membrane Subunits

Unassembled subunits in the cytosol are recognized by quality-control machinery due to the aberrant exposure of thermodynamically unfavorable subunit interfaces (Yanagitani et al., 2017). However, the biophysical properties of orphan membrane protein subunits that lead to their recognition and degradation are comparatively ill defined. We therefore tested the insertion and topology of WRB and CAML to better understand how and why they are quality control substrates when unassembled.

We first demonstrated that our *in vitro* translation and insertion system, comprised of rabbit reticulocyte lysate (RRL) supplemented with canine-derived rough microsomes (cRMs), could recapitulate the stable assembly of WRB and CAML, as observed in cells (Figure S1D). We then determined the topology of individually translated CAML and WRB by using a protease protection assay (Figure 1B). WRB adopts the expected topology where all three TMDs are efficiently inserted, resulting in the positioning of the N and C termini in the lumen and cytosol, respectively (Figure 1C; Figure S2A).

If CAML also autonomously inserts correctly, we would expect to observe two protected fragments: an untagged fragment representing TMDs 1–2 and a 3F4-tagged fragment representing TMD3. However, we do not detect any 3F4-tagged protease-protected species, suggesting that the C terminus of CAML is aberrantly localized to the cytosol (Figure 1D). As we do not detect a FLAG-tagged fragment, indicating that TMD1 is properly inserted with its N terminus in the cytosol, these observations are consistent with two possible CAML topologies: (1) one where TMDs 1 and 2 are properly inserted but TMD3 remains in the cytosol; or (2) one where TMDs 1 and 3 are inserted, but TMD2 is “skipped” and remains in the ER lumen (Figure S2B). To differentiate between these two models, we initially sought to exploit a native glycosylation site in CAML’s second loop, which would only be positioned in the ER lumen if TMD2 was skipped, as in model 2. However, further experiments suggest that this site is not accessible and, thus, cannot be used to infer the topology of CAML (data not shown). Instead, we exploited the fact that the native CAML sequence contains a single methionine residue in loop 1 (M225), which leads to incorporation of <sup>35</sup>S-methionine at this position (Figure S2B). If we make the conservative mutation M225C, the fragment remaining after protease digestion would either be completely unlabeled in the case of model 1 or retain two radioactive methionine residues (in loop 2) in model 2 (Figure S2C). As the protected fragment of CAML M225C retains at least one <sup>35</sup>S-methionine and can therefore be clearly visualized, this experiment is most consistent with model 2, where the untagged protease-protected fragment of CAML contains all three TMDs (Figure S2D). Moreover, adding a methionine to either CAML TMD2 (S250M) or TMD3 (C284M) increases the signal of the protected fragment, indicating both TMD2 and TMD3 are included within the protected fragment (Figure S2D).

Our protease protection experiments therefore support a model where, when expressed alone, the first and third TMDs of CAML insert into the lipid bilayer, whereas the second TMD is aberrantly exposed to the ER lumen. TMD3 is, thus, inserted in the incorrect orientation, with its C terminus aberrantly localized to the cytosol. This is consistent with the predicted inability of the second TMD to autonomously insert due to the presence of several charged, polar, and helix-breaking residues (Figure 1B,  $\Delta G = 1.879$ ; Hessa et al., 2007). Our biochemical evidence suggests the majority of the orphan CAML population is inserted in this manner, in contrast to previous reports in which both TMD2 and TMD3 are localized to the lumen (Carvalho et al., 2019).

We next tested whether the insertion of CAML was affected by the presence of WRB by using the appearance of the 3F4-tagged TMD3 after protease treatment as a proxy for CAML folding. Using a similar *in vitro* strategy, we observe that both co- and pre-expression of WRB results in increasing amounts of properly inserted CAML, as indicated by the appearance of a 3F4-tagged protease-protected fragment (Figure 2A; Figure S3A). When WRB is translated prior to CAML rather than simply co-expressed, we consistently observe an increase in the levels of protected TMD3, suggesting that the timing of WRB recruitment is potentially important for CAML folding. Of note, detection of the protease-protected 3F4-tagged TMD3 requires enrichment by immunoprecipitation, suggesting that, at least *in vitro*, WRB does not correctly fold all of the exogenously expressed CAML.

To confirm that WRB-dependent insertion of CAML was not an artifact of the *in vitro* system, we exploited a split GFP system to determine CAML topology in cells (Figure 2B; Figure S3; Hyun et al., 2015). We generated mammalian cell lines expressing the first 10  $\beta$ -strands of GFP in the ER lumen. Expression of constructs that position the 11th  $\beta$ -strand of GFP in the lumen, but not in the cytosol, allow for complementation with GFP<sub>1-10</sub>, and the resulting fluorescence can be measured by flow cytometry (Figures S3B and S3C). When GFP<sub>11</sub> is positioned at the C terminus of CAML, a 5-fold increase in fluorescence is observed specifically in the presence of exogenous WRB but not another unrelated membrane protein (Figure 2C). This increase in GFP fluorescence upon co-expression of CAML and WRB at the ER is striking enough to be directly visualized by fluorescence microscopy (Figure 2D). The low level of GFP complementation observed when CAML-GFP<sub>11</sub> is expressed individually may be due to partial insertion by endogenous WRB. The correct insertion of CAML's TMDs 2 and 3 is, therefore, dependent on an association with WRB both *in vitro* and in cells. These data are consistent with recent findings that describe a WRB-dependent conformational change to CAML in cells (Carvalho et al., 2019).

Taken together, these observations suggest that there are at least two distinct mechanisms for the recognition of orphan subunits at the ER. WRB, despite adopting the correct topology, is destabilized in the absence of CAML. This may be due to the presence of charged or polar residues within the TMDs that would generally be shielded at the subunit-interface with CAML. Exposure of such residues could lead to recognition of unassembled WRB by membrane-embedded quality-control machinery. WRB is, therefore, representative of a larger class of membrane protein subunits that are properly inserted and folded and, yet, are degraded by the ubiquitin-proteasome pathway when unassembled (Bañó-Polo et al., 2017; Lippincott-Schwartz et al., 1988).

Conversely, the regulation of CAML in the absence of WRB is at least partly due to the incorrect insertion of its TMD2. Mutations that decrease the hydrophobicity of CAML TMD2 stabilize overexpressed CAML (Figure 3A). The effect is slight (approximately 2-fold), which is consistent with mutant CAML remaining unassembled and misfolded, with TMD3 in the wrong orientation within the bilayer. Furthermore, the fusion of CAML TMD2 to an unrelated membrane protein results in its destabilization compared to fusion with a hydrophilic sequence of similar length (Figure 3B). Together, this suggests that the exposure of CAML TMD2 to the ER lumen is both necessary and sufficient for destabilization of unassembled CAML. Aberrant exposure of this hydrophobic segment serves as a flag for recognition, allowing CAML to recruit luminal quality control machinery for its degradation (Feige and Hendershot, 2013).

### The Timing of CAML Reorientation

Given the observation that WRB is required for CAML folding, the two most likely models are that the reorientation of TMDs 2 and 3 is happening (1) co-translationally during the synthesis of CAML at the Sec61 translocation channel or (2) post-translationally after CAML has been released from the ribosome. To discriminate between these two possibilities, we first tested whether WRB can bind nascent CAML while it is still associated with the ribosome and Sec61 (Figure 4A). Consistent with a post-translational

mechanism for insertion, we observe that CAML is able to immunoprecipitate significantly more WRB after release from the ribosome than when stalled immediately before the stop codon (Figure 4A). The observation that CAML cannot stably bind WRB prior to translation termination, when TMD3 is buried in the ribosomal exit tunnel, is consistent with the observation that TMDs1–2 of CAML are insufficient for stable recruitment of WRB, as truncation analysis demonstrates TMD3 (through residue 287) is necessary for the interaction (Figure 4B).

To further explore the mechanism of CAML folding, we exploited our ability to pre-load membranes with either CAML or WRB to control the order of translation and insertion into the membrane (Figure S4). One would predict that if the folding of CAML must occur co-translationally, TMD3 insertion would be more efficient when WRB is translated first and, thereby present throughout the synthesis of CAML. We observe a small but reproducible increase in the amount of protected CAML TMD3 when WRB is expressed first (Figure 4C), consistent with the improved folding of CAML observed upon pre-loading versus co-expression of WRB (Figure 2A).

Together, these experiments are more consistent with folding of CAML by WRB after translation termination and release from the ribosome, although they suggest that successful reorientation of TMDs2–3 may depend on the timing of WRB recruitment to nascent CAML. However, we cannot exclude the possibility that (1) WRB binding to CAML is initiated co-translationally, but that the interaction is too weak and/or transient to survive immunoprecipitation; or (2) that CAML folding occurs after release from the ribosome, but in the context of the translocon, which could potentially reduce the energetic cost of reorientation of TMDs2 and 3 across the lipid bilayer.

Taken together, we suggest a working model for the folding and assembly of the WRB/CAML complex (Figure 4D). Stable recruitment of WRB occurs after release from the ribosome and is likely mediated by the first and third TMDs of CAML. Whether this partially folded version of CAML is stabilized by either an intramembrane and/or luminal chaperone, or remains associated with Sec61 prior to binding to WRB, remains to be determined. Similarly, unassembled WRB may also require stabilization by a membrane-embedded chaperone to provide sufficient time for association with CAML. Upon binding, WRB is able to correctly reorient CAML into the ER membrane, thereby acting as an internal chaperone for the folding and assembly of the WRB/CAML complex. This strategy allows insertion of the poorly hydrophobic TMD2, which is not independently recognized by Sec61, suggesting at least one mechanism for inserting non-optimal TMDs that sit at the interface of two membrane protein subunits. The lack of certainty surrounding the complex stoichiometry means that we cannot conclude whether WRB is acting on a single CAML subunit as part of a stable complex or whether it is acting catalytically on multiple copies of CAML. Given that WRB/CAML is itself a membrane protein insertase, it is possible that this post-translational folding is a unique feature of assembly of this complex. However, evidence for other such post-translational topological changes in polytopic proteins suggests that this could be a more general mechanism used by multi-subunit complexes (Hegde and Lingappa, 1999; Lu et al., 2000; Serdiuk et al., 2016).

In the event that either CAML or WRB cannot assemble, their orphan forms are recognized and degraded by the ubiquitin-proteasome pathway. This recognition occurs by two distinct mechanisms: (1) improperly folded CAML aberrantly exposes its TMD2 to the ER lumen, which makes it a target for the luminal quality-control machinery; and (2) WRB, although folded correctly, must be recognized due to the aberrant exposure of its subunit interface within the lipid bilayer. As eukaryotic membrane protein subunits differ enormously in size, topology, and the biophysical properties of their exposed interfaces, interaction with such a diverse range of substrates would require a network of chaperones in the ER membrane that remain to be identified. This work sets the stage for future research to determine both the triage factors that target unassembled proteins toward either a biosynthetic or degradative fate and how these pathways are coordinated to ensure the precise assembly of multi-subunit complexes at the ER.

## STAR★METHODS

Detailed methods are provided in the online version of this paper and include the following:

### LEAD CONTACT AND MATERIALS AVAILABILITY

Further information and requests for resources and reagents should be directed to and will be fulfilled by the Lead Contact, Rebecca Voorhees (voorhees@caltech.edu). All unique/stable reagents generated in this study are available from the Lead Contact with a completed Material Transfer Agreement.

### EXPERIMENTAL MODEL AND SUBJECT DETAILS

Flp-In 293 T-Rex cells (female) were maintained in Dulbecco's Modified Eagle's Medium (DMEM) with 10% fetal calf serum (FCS) in the presence of 15 µg/mL blasticidin and 100 µg/ml hygromycin. Cells were grown at 5% CO<sub>2</sub> and at 37°C.

### METHOD DETAILS

**Constructs**—Constructs for expression in cultured mammalian cells were generated in either the pcDNA5/FRT/TO (Thermo Scientific) or pcDNA3.1 backbone. To create the fluorescent reporters described in Figure 1A, cDNA for human CAML [(cDNA)*CAMLG*] and WRB [(cDNA)*GET1*] was purchased from IDT and inserted into a pcDNA5 vector expressing GFP-2A-RFP resulting in an N- (CAML) or C-terminal (WRB) GFP fusion. In order to express the split GFP<sub>1-10</sub> in the ER lumen, a construct expressing the human calreticulin signal sequence preceding a GFP<sub>1-10</sub>-KDEL was also generated in pcDNA5 (Cabantous et al., 2005; Kamiyama et al., 2016). WRB-BFP, the turkey β<sub>1</sub>-adrenergic receptor, CAML-GFP<sub>11</sub> (GFP<sub>11</sub> tag: RDHMLVHEHYVNAAGIT), cytosolic RFP-2A-GFP<sub>11</sub>, and RFP-2A-VAMP-GFP<sub>11</sub> were inserted into pcDNA3.1 for transient mammalian expression. All experiments were performed in the Flp-In T-REx 293 cell line (Thermo Scientific). The mCherry and mEGFP versions of RFP and GFP are used throughout this manuscript, though are referred to as RFP and GFP for simplicity in the text and figures.

Constructs for expression in rabbit reticulocyte lysate (RRL) were based on the SP64 vector (Promega). For all protease protection assays (Figures 1C, 1D, 2A, and 4C) CAML was

expressed with an N-terminal 3xFLAG tag and a C-terminal 3F4-tag (Stefanovic and Hegde, 2007) while WRB was appended with an N-terminal 1xHA tag and C-terminal 3F4 tag (except in Figure S2A, where WRB is C-terminally 3xFLAG tagged). Tags were chosen to minimize interference with TMD insertion, with tags containing multiple charged or polar residues being placed on the cytosolic face.

**Cell culture**—Stable cell lines expressing GFP-CAML-2A-RFP, WRB-GFP-2A-RFP, or ER GFP<sub>1–10</sub> were generated using the Flp-In T-Rex 293 Cell Line (Thermo Scientific) according to the manufacturer's instructions. In brief, a 10 cm dish of cells was transfected with 9 µg of Flp-Recombinase (plasmid pOG44) and 1 µg of a specific pcDNA5/FRT plasmid using TransIT-293 transfection reagent (Mirus, MIR2705). 48 hours after transfection, cells were selected with 100 µg/mL hygromycin in DMEM media containing 10% fetal bovine serum and 15 µg/mL blasticidin. After 7–10 days the resulting isogenic cell population was expanded for maintenance and preservation.

For overexpression of GFP-tagged CAML and WRB (Figure S1C), cells were cultured in 6-well tissue culture plates, induced with 1 µg/mL doxycycline for 24 to 72 hours, and harvested in 5 mM EDTA pH 8.0 in 1X PBS. Cells were lysed with NETN lysis buffer (250 mM NaCl, 5 mM EDTA pH 8.0, 50 mM Tris-HCl pH 8.0, 0.5% IGEPAL CA-630, 1X protease inhibitors) for 1 hour at 4°C. Cell lysates were used directly for analysis by western blot. Samples were normalized by cell counting prior to lysis.

**Purification from cells**—Purification of GFP-tagged CAML and WRB from mammalian cells were performed using an anti-GFP nanobody (Kirchhofer et al., 2010; Pleiner et al., 2015). Briefly, cell lines of GFP-2A-RFP, WRB-GFP-2A-RFP, and GFP-CAML-2A-RFP were cultured in 10 cm dishes until 70% confluent, induced with 1 mg/mL doxycycline and harvested after 24 hours. Cells were lysed in Solubilization Buffer (50 mM HEPES pH 7.5, 200 mM KOAc, 2 mM MgOAc<sub>2</sub>, 1 % Digitonin, 1X protease inhibitors, 1 mM DTT) for 20 minutes at 4°C. Pierce Streptavidin Magnetic Beads (Thermo Scientific, 88817) were equilibrated with 3.75 µg biotinylated anti-GFP nanobody in wash buffer (50 mM HEPES pH 7.5, 100 mM KOAc, 2 mM MgOAc<sub>2</sub>, 0.25% Digitonin, 1 mM DTT). Cell lysates were incubated with anti-GFP nanobody immobilized on Streptavidin support for one hour at 4°C. GFP-tagged proteins were eluted with 0.5 µM SUMOstar protease and used directly for western blot analysis.

**Western blot analysis**—Antibodies were purchased against CAML (Synaptic Systems, 359 002), WRB (Synaptic Systems, 324 002), and α-tubulin (Sigma, T9026). The antibody against the 3F4 epitope was a gift from the Hegde lab and has been previously described (Chakrabarti and Hegde, 2009). Secondary antibodies used were HRP-conjugated Goat Anti-Rabbit (BioRad, 170–6515) and Anti-Mouse (BioRad, 172–1011). Anti-FLAG (A2220) and HA resin (A2095) were obtained from Sigma (St. Louis, MO). Pre-designed Silencer Select siRNAs from Thermo Fisher were obtained for CAML (s2370, s2371, s2372) and WRB (s14904, s14905).

**Flow Cytometry**—All siRNA experiments (Figure 1A) were performed in a 6-well tissue culture plate. Cells were transfected with 3 ng of siRNA per well using RNAiMAX

lipofectamine (ThermoFisher, 13778150). After 48 hours, the integrated reporter gene was induced with 1  $\mu\text{g}/\text{mL}$  doxycycline for 24 hours. Live cells were first incubated with trypsin before collection, pelleted, and resuspended in 300  $\mu\text{L}$  of PBS containing 1  $\mu\text{M}$  Sytox Blue Dead Cell Stain (ThermoFisher, S34857) and analyzed on a Miltenyi Biotec MACSQuant VYB Flow Cytometer. Data analysis for all flow cytometry experiments was performed using the FloJo software package.

**GFP complementation assays**—GFP complementation experiments by flow cytometry were performed in a 6-well tissue culture plate. Expression of the GFP<sub>1–10</sub> protein was induced for 72 hours with 1  $\mu\text{g}/\text{mL}$  doxycycline before transfection of 0.17  $\mu\text{g}$  of GFP-n constructs, 0.17  $\mu\text{g}$  of WRB-BFP or  $\beta_1\text{AR}$ -BFP, and 1.36  $\mu\text{g}$  of pcDNA3.1 backbone with TransIT-293 transfection reagent. Cells were harvested and analyzed by flow cytometry 24 hours after transfection. For analysis by confocal microscopy, the cells were grown in a 24-well tissue culture plate containing 12 mm glass coverslips coated in poly-D-lysine. The induction and transfection conditions for imaged samples were identical as those subjected to flow cytometry, except cells were transfected with 30 ng of RFP-2A-CAML-GFP-n, 30 ng of BFP or WRB-BFP and 240 ng of pcDNA3.1 backbone. The cells were fixed for fluorescence microscopy according to standard protocol. In brief, the cells were washed with PBS before being incubated with 3.6% paraformaldehyde for 30 minutes. The cells were washed again, treated with Prolong Diamond Antifade Mountant (ThermoFisher, P36961) and sealed onto a slide. Imaging was performed using an LSM 800 confocal microscope (Zeiss).

**Mammalian *in vitro* translation**—Translation extracts were prepared using nucleated rabbit reticulocyte lysate (RRL) and canine derived pancreatic microsomes (cRMs) as previously described (Sharma et al., 2010; Walter and Blobel, 1983). Briefly, templates for *in vitro* transcription were generated by PCR using primers that included the SP6 promoter at the 5' end and a stop codon followed by a short untranslated region at the 3' end. In the case of Figures 4A and 4B, primers were designed to anneal upstream of the stop codon in order to generate a truncated protein product in which the C-terminal residue is a valine, known to stabilize the peptidyl-tRNA product (Shao et al., 2013). Transcription reactions were incubated at 37°C for 1 hour, and then used directly in a translation reaction, which was incubated for 35 minutes at 32°C. Where stated, puromycin was added to a final concentration of 1 mM and samples were incubated at 32°C for a further 10 minutes.

To generate pre-loaded membranes of either WRB or CAML, as used in Figures 2A, 4B, and 4C, cRMs were included in an initial translation reaction for 12 minutes with the respective mRNA. Membranes were purified by pelleting for 20 minutes at 55,000 rpm in a TLA55 at 4°C through a 20% sucrose cushion in physiological salt buffer (50 mM HEPES pH 7.5, 100 mM KOAc, 2 mM MgOAc<sub>2</sub>). Pellets were resuspended in physiological salt buffer at a concentration of A<sub>280</sub> ~80. Membranes were either used directly in a second translation/insertion reaction or aliquoted and flash frozen for storage at –80°C. We saw no reduction in translation and insertion efficiency after freezing.

**Proteinase K digestion**—Protease digestions were performed on ice by addition of 0.5 mg/mL proteinase K to translation reactions and incubated for an additional hour. The

digestion was quenched by addition of 5 mM PMSF in DMSO, followed by transfer to boiling 1% SDS in 0.1 M Tris pH 8.0 (room temperature). Immunoprecipitation of protected fragments was performed in IP buffer (50 mM HEPES pH 7.5, 100 mM KOAc, 2 mM MgOAc<sub>2</sub>, and 1% Triton X-100).

**Co-immunoprecipitation assays**—Co-immunoprecipitation experiments (Figures 4A, 4B, and S1D) were performed by setting up translation reactions in the presence of cRMs, and then purifying the membranes via pelleting for 20 minutes at 55,000 rpm in a TLA55 at 4°C through a 20% sucrose cushion in physiological salt buffer. The pellets were resuspended in physiological salt buffer before solubilization of the membranes in 1% digitonin. The samples were incubated on ice for 10 minutes, before being centrifuged for 15 minutes at 55,000 rpm in aTLA55at4°C. The subsequent supernatants were then diluted four-fold and immunoprecipitated with anti-FLAG resin.

## QUANTIFICATION AND STATISTICAL ANALYSIS

**Flow cytometry**—For Figure S1B, GFP:RFP ratios were calculated in triplicate, and normalized to the GFP-2A-RFPcell line (= 1). The mean ± standard deviations are shown (n = 3).

**Image quantification**—In Figures 2A and 4C, the amount of protected TMD3–3F4 was quantified in ImageJ by inverting the image, subtracting background, then normalizing the values to the total amount of CAML present.

## DATA AND CODE AVAILABILITY

This study did not generate any datasets or codes.

## Supplementary Material

Refer to Web version on PubMed Central for supplementary material.

## ACKNOWLEDGMENTS

We thank T. Pleiner for help with GFP affinity purification and the Caltech Flow Cytometry facility for their help with fluorescence-activated cell sorting (FACS) experiments. Confocal imaging was performed in the Caltech Biological Imaging Facility, with the support of the Caltech Beckman Institute and the Arnold and Mabel Beckman Foundation. The antibody against 3F4 was a kind gift from Ramanujan S. Hegde. This work was supported by the Heritage Medical Research Institute, the Kinship Foundation, the Pew-Stewart Foundation, and the National Institutes of Health National Institute of General Medical Sciences under award number DP2GM137412.

## REFERENCES

- Bañó-Polo M, Martínez-Garay CA, Grau B, Martínez-Gil L, and Mingarro I (2017). Membrane insertion and topology of the translocon-associated protein (TRAP) gamma subunit. *Biochim. Biophys. Acta Biomembr* 1859, 903–909. [PubMed: 28132902]
- Béguin P, Hasler U, Beggah A, Horisberger J-D, and Geering K (1998). Membrane integration of Na,K-ATPase alpha-subunits and beta-subunit assembly. *J. Biol. Chem* 273, 24921–24931. [PubMed: 9733799]
- Bonifacino JS, Cosson P, and Klausner RD (1990). Colocalized transmembrane determinants for ER degradation and subunit assembly explain the intracellular fate of TCR chains. *Cell* 63, 503–513. [PubMed: 2225064]

- Bonifacino JS, Cosson P, Shah N, and Klausner RD (1991). Role of potentially charged transmembrane residues in targeting proteins for retention and degradation within the endoplasmic reticulum. *EMBO J.* 10, 2783–2793. [PubMed: 1915263]
- Cabantous S, Terwilliger TC, and Waldo GS (2005). Protein tagging and detection with engineered self-assembling fragments of green fluorescent protein. *Nat. Biotechnol.* 23, 102–107. [PubMed: 15580262]
- Carvalho HJF, Del Bondio A, Maltecca F, Colombo SF, and Borgese N (2019). The WRB Subunit of the Get3 Receptor is Required for the Correct Integration of its Partner CAML into the ER. *Sci. Rep.* 9, 11887. [PubMed: 31417168]
- Chakrabarti O, and Hegde RS (2009). Functional depletion of mahogunin by cytosolically exposed prion protein contributes to neurodegeneration. *Cell* 137, 1136–1147. [PubMed: 19524515]
- Colombo SF, Cardani S, Maroli A, Vitiello A, Soffientini P, Crespi A, Bram RF, Benfante R, and Borgese N (2016). Tail-anchored protein insertion in mammals function and reciprocal interactions of the two subunits of the TRC40 receptor. *J. Biol. Chem.* 291, 15292–15306. [PubMed: 27226539]
- Dephoure N, Hwang S, O’Sullivan C, Dodgson SE, Gygi SP, Amon A, and Torres EM (2014). Quantitative proteomic analysis reveals posttranslational responses to aneuploidy in yeast. *eLife* 3, e03023. [PubMed: 25073701]
- Feige MJ, and Hendershot LM (2013). Quality control of integral membrane proteins by assembly-dependent membrane integration. *Mol. Cell* 51, 297–309. [PubMed: 23932713]
- Guna A, Volkmar N, Christianson JC, and Hegde RS (2018). The ER membrane protein complex is a transmembrane domain insertase. *Science* 359, 470–73. [PubMed: 29242231]
- Harper JW, and Bennett EJ (2016). Proteome complexity and the forces that drive proteome imbalance. *Nature* 537, 328–338. [PubMed: 27629639]
- Hegde RS, and Lingappa VR (1999). Regulation of protein biogenesis at the endoplasmic reticulum membrane. *Trends Cell Biol.* 9, 132–137. [PubMed: 10203789]
- Hessa T, Meindl-Beinker NM, Bernsel A, Kim H, Sato Y, Lerch-Bader M, Nilsson I, White SH, and von Heijne G (2007). Molecular code for trans-membrane-helix recognition by the Sec61 translocon. *Nature* 450, 1026–1030. [PubMed: 18075582]
- Huttlin EL, Bruckner RJ, Paulo JA, Cannon JR, Ting L, Baltier K, Colby G, Gebreab F, Gygi MP, Parzen H, et al. (2017). Architecture of the human interactome defines protein communities and disease networks. *Nature* 545, 505–509. [PubMed: 28514442]
- Hyun SI, Maruri-Avidal L, and Moss B (2015). Topology of Endoplasmic Reticulum-Associated Cellular and Viral Proteins Determined with Split-GFP. *Traffic* 16, 787–795. [PubMed: 25761760]
- Itakura E, Zavodszky E, Shao S, Wohlever ML, Keenan RJ, and Hegde RS (2016). Ubiquilins Chaperone and Triage Mitochondrial Membrane Proteins for Degradation. *Mol. Cell* 63, 21–33. [PubMed: 27345149]
- Juszkiewicz S, and Hegde RS (2017). Initiation of Quality Control during Poly(A) Translation Requires Site-Specific Ribosome Ubiquitination. *Mol. Cell* 65, 743–750.e4. [PubMed: 28065601]
- Juszkiewicz S, and Hegde RS (2018). Quality Control of Orphaned Proteins. *Mol. Cell* 71, 443–457. [PubMed: 30075143]
- Kamiyama D, Sekine S, Barsi-Rhyne B, Hu J, Chen B, Gilbert LA, Ishikawa H, Leonetti MD, Marshall WF, Weissman JS, and Huang B (2016). Versatile protein tagging in cells with split fluorescent protein. *Nat. Commun.* 7, 11046. [PubMed: 26988139]
- Kirchhofer A, Helma J, Schmidhals K, Frauer C, Cui S, Karcher A, Pellis M, Muylderms S, Casas-Delucchi CS, Cardoso MC, et al. (2010). Modulation of protein properties in living cells using nanobodies. *Nat. Struct. Mol. Biol.* 17, 133–138. [PubMed: 20010839]
- Lippincott-Schwartz J, Bonifacino JS, Yuan LC, and Klausner RD (1988). Degradation from the endoplasmic reticulum: disposing of newly synthesized proteins. *Cell* 54, 209–220. [PubMed: 3292055]
- Lu Y, Turnbull IR, Bragin A, Carveth K, Verkman AS, and Skach WR (2000). Reorientation of aquaporin-1 topology during maturation in the endoplasmic reticulum. *Mol. Biol. Cell* 11, 2973–2985. [PubMed: 10982394]
- Marsh JA, and Teichmann SA (2015). Structure, dynamics, assembly, and evolution of protein complexes. *Annu. Rev. Biochem.* 84, 551–575. [PubMed: 25494300]

- Minami Y, Weissman AM, Samelson LE, and Klausner RD (1987). Building a multichain receptor: synthesis, degradation, and assembly of the T-cell antigen receptor. *Proc. Natl. Acad. Sci. USA* 84, 2688–2692. [PubMed: 3495001]
- Pleiner T, Bates M, Trakhanov S, Lee CT, Schliep JE, Chug H, Böhning M, Stark H, Urlaub H, and Görlich D (2015). Nanobodies: site-specific labeling for super-resolution imaging, rapid epitope-mapping and native protein complex isolation. *eLife* 4, e11349. [PubMed: 26633879]
- Rapoport TA (2007). Protein translocation across the eukaryotic endoplasmic reticulum and bacterial plasma membranes. *Nature* 450, 663–669. [PubMed: 18046402]
- Rivera-Monroy J, Musiol L, Unthan-Fechner K, Farkas Á, Clancy A, Coy-Vergara J, Weill U, Gockel S, Lin SY, Corey DP, et al. (2016). Mice lacking WRB reveal differential biogenesis requirements of tail-anchored proteins in vivo. *Sci. Rep* 6, 39464. [PubMed: 28000760]
- Schneider CA, Rasband WS, and Eliceiri KW (2012). NIH Image to ImageJ: 25 years of Image Analysis. *Nat. Methods* 9, 671–675. [PubMed: 22930834]
- Serdiuk T, Balasubramaniam D, Sugihara J, Mari SA, Kaback HR, and Müller DJ (2016). YidC assists the stepwise and stochastic folding of membrane proteins. *Nat. Chem. Biol* 12, 911–917. [PubMed: 27595331]
- Shao S, von der Malsburg K, and Hegde RS (2013). Listerin-dependent nascent protein ubiquitination relies on ribosome subunit dissociation. *Mol. Cell* 50, 637–648. [PubMed: 23685075]
- Sharma A, Mariappan M, Appathurai S, and Hegde RS (2010). *In vitro* dissection of protein translocation into the mammalian endoplasmic reticulum. *Methods Mol. Biol* 619, 339–363. [PubMed: 20419420]
- Shemorry A, Hwang CS, and Varshavsky A (2013). Control of protein quality and stoichiometries by N-terminal acetylation and the N-end rule pathway. *Mol. Cell* 50, 540–551. [PubMed: 23603116]
- Shiber A, Döring K, Friedrich U, Klann K, Merker D, Zedan M, Tippmann F, Kramer G, and Bukau B (2018). Cotranslational assembly of protein complexes in eukaryotes revealed by ribosome profiling. *Nature* 561, 268–272. [PubMed: 30158700]
- Shing JC, Lindquist LD, Borgese N, and Bram RJ (2017). CAML mediates survival of Myc-induced lymphoma cells independent of tail-anchored protein insertion. *Cell Death Discov* 3, 16098. [PubMed: 28580168]
- Stefanovic S, and Hegde RS (2007). Identification of a targeting factor for posttranslational membrane protein insertion into the ER. *Cell* 128, 1147–1159. [PubMed: 17382883]
- Sung MK, Porras-Yakushi TR, Reitsma JM, Huber FM, Sweredoski MJ, Hoelz A, Hess S, and Deshaies RJ (2016). A conserved quality-control pathway that mediates degradation of unassembled ribosomal proteins. *eLife* 5, 1–28.
- Vilardi F, Lorenz H, and Dobberstein B (2011). WRB is the receptor for TRC40/Asn1-mediated insertion of tail-anchored proteins into the ER membrane. *J. Cell Sci* 124, 1301–1307. [PubMed: 21444755]
- Vilardi F, Stephan M, Clancy A, Janshoff A, and Schwappach B (2014). WRB and CAML are necessary and sufficient to mediate tail-anchored protein targeting to the ER membrane. *PLoS One* 9, e85033. [PubMed: 24392163]
- Volkmar N, Thezenas ML, Louie SM, Juszkiwicz S, Nomura DK, Hegde RS, Kessler BM, and Christianson JC (2019). The ER membrane protein complex promotes biogenesis of sterol-related enzymes maintaining cholesterol homeostasis. *J. Cell Sci* 132, jcs223453.
- Walter P, and Blobel G (1983). Preparation of microsomal membranes for cotranslational protein translocation. *Methods Enzymol.* 96, 84–93. [PubMed: 6656655]
- Wang F, Chan C, Weir NR, and Denic V (2014). The Get1/2 transmembrane complex is an endoplasmic-reticulum membrane protein insertase. *Nature* 512, 441–444. [PubMed: 25043001]
- Xu Y, Anderson DE, and Ye Y (2016). The HECT domain ubiquitin ligase HUWE1 targets unassembled soluble proteins for degradation. *Cell Discov.* 2, 16040. [PubMed: 27867533]
- Yamamoto Y, and Sakisaka T (2012). Molecular machinery for insertion of tail-anchored membrane proteins into the endoplasmic reticulum membrane in mammalian cells. *Mol. Cell* 48, 387–397. [PubMed: 23041287]
- Yanagitani K, Juszkiwicz S, and Hegde RS (2017). UBE2O is a quality control factor for orphans of multiprotein complexes. *Science* 357, 472–475. [PubMed: 28774922]

### Highlights

- Unassembled subunits of membrane protein complexes must be recognized and degraded
- The obligate hetero-oligomer WRB/CAML has differential modes of orphan recognition
- WRB is inserted correctly independently of CAML but is degraded when unassembled
- CAML requires WRB to fold correctly, which prevents exposure of a degra

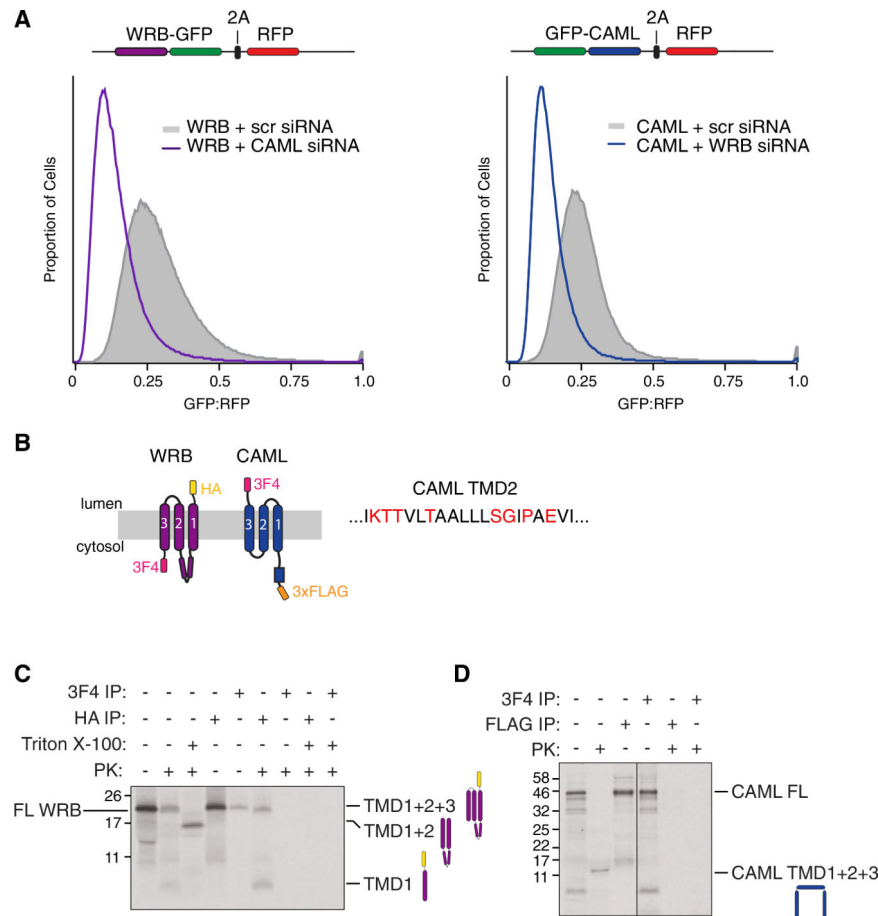


**Figure 1. Characterization of Orphaned CAML and WRB**

(A) Histograms of CAML and WRB overexpression in HEK293T mammalian cells, as determined by flow cytometry. siRNA knockdown of their respective binding partners results in a decrease in the GFP:RFP ratio for both CAML and WRB. The data shown are representative of three biological replicates.

(B) Schematic depicting the expected correct topology of WRB and CAML, along with the epitope tags used for *in vitro* translation. The sequence of the second TMD of CAML is shown, with polar, charged, and helix-breaking residues highlighted.

(C) <sup>35</sup>S-methionine-labeled hemagglutinin (HA)-WRB-3F4 was translated in rabbit reticulocyte lysate (RRL) in the presence of canine-derived rough microsomes (cRMs). The total products were treated with proteinase K (PK) in the presence or absence of detergent and then analyzed directly or following immunoprecipitation by the 3F4 or HA tag. WRB adopts the expected topology, with the N and C termini in the lumen and cytosol, respectively. The coiled-coil domain between TMD1 and TMD2 partially protects the loop from cleavage by PK, giving two major HA-tagged species in the absence of detergent. Upon the addition of detergent, the loop between TMD2 and TMD3 is cleaved, resulting in the loss of the HA tag. Replacing the C-terminal 3F4 tag with a larger 3xFLAG tag results in a larger change in molecular weight, consistent with the ~20kDa band after PK treatment, representing a fragment +3 lacking the C terminus (Figure S2A). See also Figure S2.

(D) Similar to (C) but for the for the FLAG-CAML-3F4 construct. There is an untagged protease-protected fragment present that likely corresponds to TMDs1–3 of CAML. The lack of a protease-protected 3F4 fragment demonstrates that the C terminus of CAML remains aberrantly exposed to the cytosol. In each case, three biological replicates were performed.

Author Manuscript

Author Manuscript

Author Manuscript

Author Manuscript

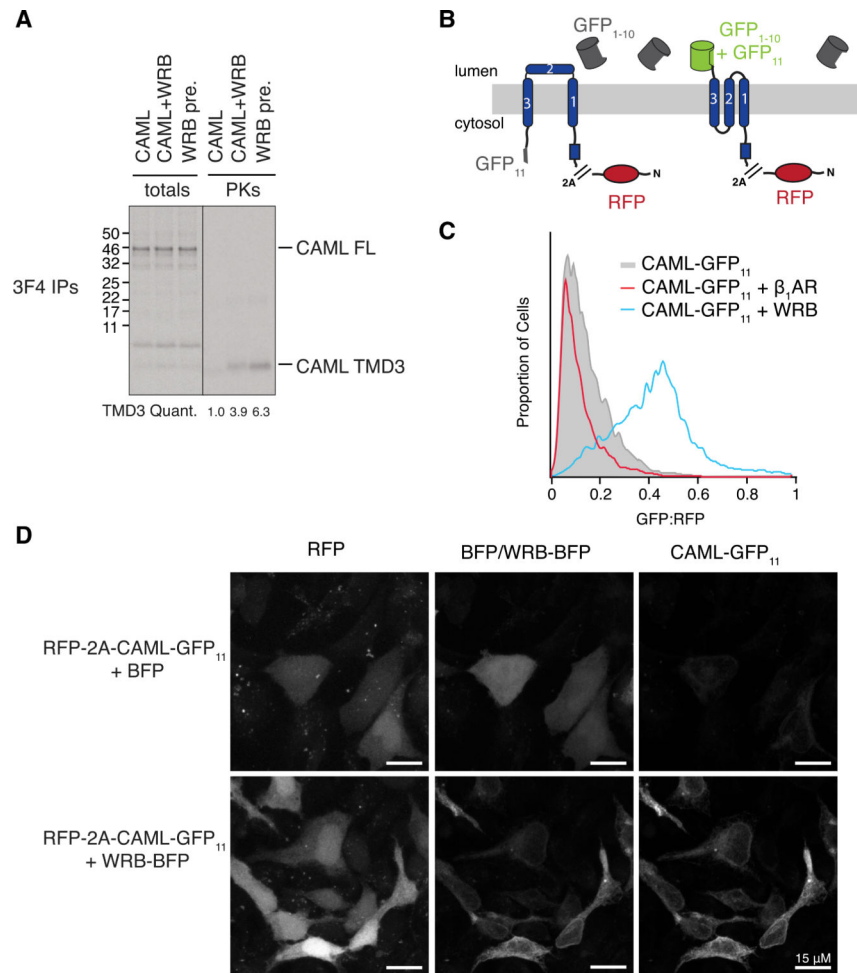


### Figure 2. CAML Requires WRB for Correct Insertion

(A)  $^{35}\text{S}$ -methionine-labeled FLAG-CAML-3F4 was translated in RRL in the presence of cRMs either individually, alongside WRB, or with cRMs pre-loaded with WRB. Following digestion with PK, total translations and digested reactions were immunoprecipitated by the 3F4 epitope tag. The positions of bands corresponding to full-length (FL) CAML and CAML TMD3 are indicated. The amount of protected CAML TMD3 relative to total translated protein is indicated. Corresponding amounts of WRB present are shown in Figure S3A.

(B) Schematic illustrating the split GFP system used to establish the topology of CAML in cells. CAML containing the 11th  $\beta$  strand of GFP (GFP<sub>11</sub>) at its C terminus was transfected into cells stably expressing the remainder of GFP (GFP<sub>1-10</sub>) in the ER lumen. The correct insertion of CAML TMD3 would localize GFP<sub>11</sub> to the ER lumen, resulting in complementation and GFP fluorescence. See also Figure S3.

(C) Flow cytometry analysis of the system described in (B) for RFP-2A-CAML-GFP<sub>11</sub> expressed either alone or alongside an unrelated membrane protein ( $\beta_1\text{AR}$ -BFP) or WRB-BFP.

(D) ER GFP<sub>1-10</sub>-expressing cells were co-transfected with RFP-2A-CAML-GFPn and BFP or WRB-BFP. Fixed cells were then imaged by confocal microscopy. The scale bar in each image represents 15  $\mu$ M. Three biological replicates were performed for all experiments.

Author Manuscript

Author Manuscript

Author Manuscript

Author Manuscript

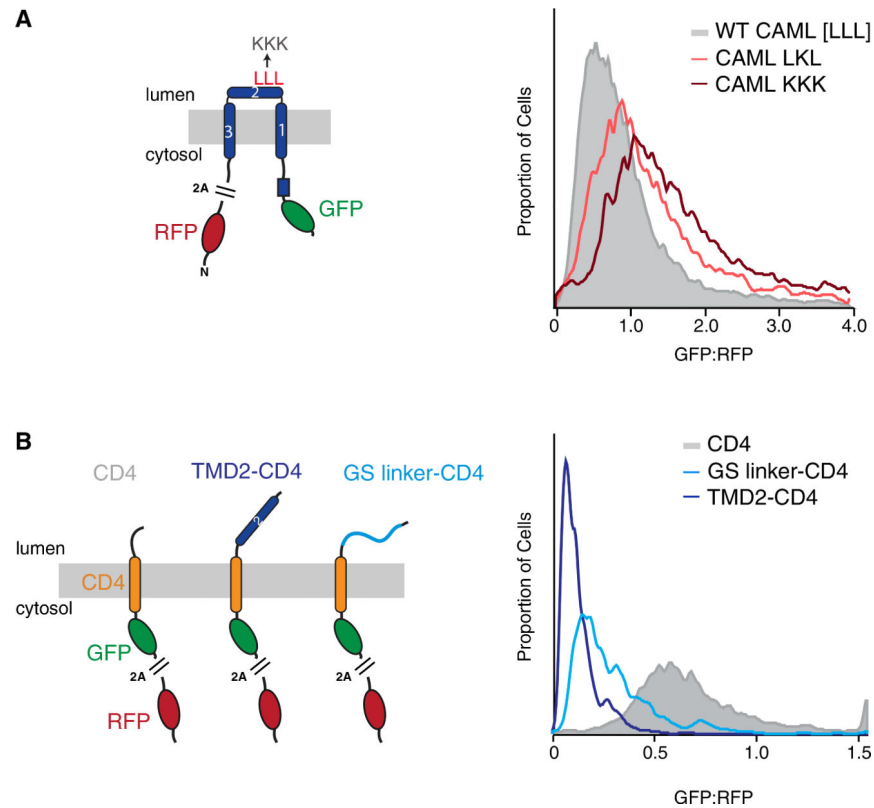


**Figure 3. Localization of CAML TMD2 to the ER Lumen Is Both Necessary and Sufficient for Degradation of Orphan CAML**

(A) Orphan CAML degradation is contingent on the hydrophobicity of its TMD2, which is aberrantly exposed to the ER lumen. Mutation of either one (L248K), or three (L247K, L248K, and L249K) leucine residues within TMD2 has a stabilizing effect on overexpressed CAML, with the triple mutation resulting in approximately a 2-fold stabilization over the wild type.

(B) Fusion constructs of the CD4 TMD-GFP with either CAML TMD2 or a length-matched glycine-serine linker were targeted to the ER by using the prolactin signal sequence. The stability of each construct was determined using flow cytometry as previously described. Two biological replicates were performed in each case.

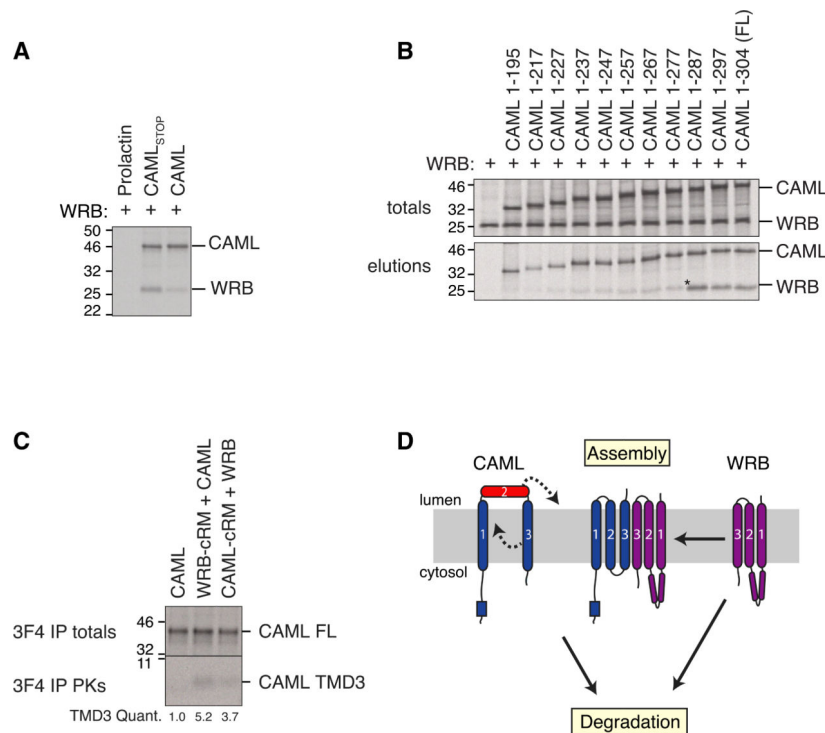


**Figure 4. WRB Causes Reorientation of CAML TMD2–3 following Release from the Ribosome**

(A) <sup>35</sup>S-methionine labeled FL FLAG-CAML with or without a stop codon (or an untagged control) was produced under conditions that maintain the peptidyl-tRNA linkage in the presence of cRMs preloaded with WRB. The membranes were solubilized, and complexes were affinity purified by the FLAG tag of CAML.

(B) <sup>35</sup>S-methionine-labeled CAML truncations were translated in the presence of WRB-preloaded cRMs, and the reactions were treated with puromycin to release the truncated nascent chains from the ribosome. Solubilized complexes were affinity purified under native conditions by the FLAG tag of CAML. The minimal CAML truncation required to stably immunoprecipitate WRB is indicated with an asterisk.

(C) cRMs were introduced during the translation of either (1) no transcript, (2) CAML-3F4, or (3) WRB to produce (1) empty, (2) <sup>35</sup>S-methionine-labeled WRB-preloaded membranes, or (3) <sup>35</sup>S-methionine-labeled CAML-3F4-preloaded membranes. Membranes were purified before being used in a second round of translation to produce <sup>35</sup>S-methionine-labeled CAML-3F4 or WRB. Protection of CAML TMD3, as a proxy for CAML folding, was analyzed using a protease protection assay and immunoprecipitation by the 3F4 tag as described in Figure 2A. The amount of protected CAML TMD3 relative to total translated CAML is indicated. Three biological replicates were performed for all experiments. See also Figure S4.

(D) A proposed model for the regulation of assembly of the WRB/CAML complex: upon initial synthesis, CAML is misfolded, aberrantly localizing TMD2 to the ER lumen. The post-translational recruitment of WRB then allows CAML to insert and fold correctly. For simplicity, we have depicted a single WRB/CAML heterodimeric interaction, but WRB may operate catalytically to fold multiple CAML subunits to account for the observed excess of CAML relative to WRB (Colombo et al., 2016). In the absence of WRB, TMD2 serves as a

flag for degradation of orphaned CAML, which can exploit the luminal quality-control machinery for recognition and degradation. In contrast, WRB independently adopts the correct topology upon synthesis and, yet, is robustly degraded in the absence of CAML. Together, WRB and CAML therefore represent two distinct mechanisms for stoichiometric regulation within the ER membrane.

Author Manuscript

Author Manuscript

Author Manuscript

Author Manuscript

## KEY RESOURCES TABLE

REAGENT or RESOURCE	SOURCE	IDENTIFIER
Antibodies		
Rabbit polyclonal anti-CAML	Synaptic Systems	Cat. #359 002, RRID:AB_2620118
Rabbit polyclonal anti-WRB	Synaptic Systems	Cat. #324 002, RRID:AB_2620063
Rabbit polyclonal anti-GFP	Gift from Hegde lab (Chakrabarti and Hegde, 2009)	N/A
Rabbit polyclonal anti-3F4	Gift from Hegde lab (Chakrabarti and Hegde, 2009)	N/A
Mouse monoclonal anti- $\alpha$ -tubulin	Sigma-Aldrich	Cat. #T9026, RRID:AB_477593
HRP-conjugated goat anti-rabbit	BioRad	Cat. #170-6515, RRID:AB_11125142
HRP-conjugated goat anti-mouse	BioRad	Cat. #172-1011, RRID:AB_11125936
Chemicals, Peptides, and Recombinant Proteins		
Anti-GFP nanobody	(Kirchhofer et al., 2010; Pleiner et al., 2015)	N/A
Doxycycline	Sigma-Aldrich	Cat. #D9891; CAS: 24390-14-5
Digitonin	Millipore	Cat. #300410; CAS: 11024-24-1
Complete EDTA-free protease inhibitor cocktail	Roche	Cat. #11873580001
Pierce Streptavidin Magnetic Beads	Thermo Scientific	Cat. #88817
SUMOstar protease	Pleiner et al., 2015	N/A
Anti-Flag M2 affinity resin	Sigma-Aldrich	Cat. #A2220
Anti-HA agarose	Sigma-Aldrich	Cat. #A2095
RNasin	Promega	Cat. #N251
SP6 Polymerase	New England Biolabs	Cat. #M0207L
EasyTag L-[35S]-Methionine	Perkin Elmer	Cat. #NEG709A005MC
S7 Micrococcal Nuclease	Roche	Cat. #10107921001
Proteinase K	Roche	Cat. # 3115836001
PMSF	Thermo Scientific	Cat. #36978
Hygromycin B	Millipore	Cat. #400051-100KU CAS: 31282-04-9
Blasticidin S	Santa Cruz Biotechnology	Cat. #sc204655 CAS: 3513-03-9
MG132 Proteasomal Inhibitor	Calbiochem	Cat. #474790
Sytox Blue Dead Cell Stain	Thermo Scientific	Cat. #34857
Poly-D-lysine	GIBCO	Cat. # A3890401
Paraformaldehyde	Electron Microscopy Sciences	Cat. #15714
Prolong Diamond Antifade Mountant	Thermo Scientific	Cat. #P36961
Experimental Models: Cell Lines		
Flp-In T-REx 293 cell line	Thermo Scientific	Cat. #R78007, RRID: CVCL_U421
Oligonucleotides		
Silencer Select siRNA against CAML: GCACUUCUAUUGUCGGGAAt	Thermo Scientific	Cat. #s2370

REAGENT or RESOURCE	SOURCE	IDENTIFIER
Silencer Select siRNA against CAML: CGAUCAAUGGAUACCCUAUAtt	Thermo Scientific	Cat. #s2371
Silencer Select siRNA against CAML: GCGCGGAAGAAGAAAGUCAtt	Thermo Scientific	Cat. #s2372
Silencer Select siRNA against WRB: CGGAUAAGCUCAAAACCCAtt	Thermo Scientific	Cat. #s14904
Silencer Select siRNA against WRB: CAGUCAACAUGAUGGACGAtt	Thermo Scientific	Cat. #s14905
Primer: SP64 5' Fwd: TCATACACATACGATTTAGG	Sharma et al., 2010	N/A
Primer: SP64 Rev: CAATACGCAAACCGCCTC	Sharma et al., 2010	N/A
Recombinant DNA		
pcDNA5/FRT/TO	Thermo Scientific	Cat. #V652020
mEGFP-CAML-P2A-mCherry in pcDNA5/FRT/TO	This paper	N/A
WRB-mEGFP-P2A-mCherry in pcDNA5/FRT/TO	This paper	N/A
Calreticulin signal sequence-mEGFP <sub>1-10</sub> -KDEL in pcDNA5/FRT/TO	Cabantous et al., 2005; Kamiyama et al., 2016	N/A
pcDNA3.1	Thermo Scientific	Cat. #V79020
WRB-BFP in pcDNA3.1	This paper	N/A
Turkey $\beta_1$ AR in pcDNA3.1	This paper	N/A
mCherry-P2A-CAML-mEGFP <sub>11</sub> (sequence: RDHMLVHEHYVNAAGIT) in pcDNA3.1	This paper	N/A
mCherry-P2A-mEGFP <sub>11</sub> in pcDNA3.1	This paper	N/A
mCherry-P2A-VAMP-mEGFP <sub>11</sub> in pcDNA3.1	This paper	N/A
Flp-Recombinase pOG44	Thermo Scientific	Cat # V600520
SP64 vector	Promega	Cat #P1241
3xFLAG-CAML-3F4 in SP64	This paper	N/A
1xHA-WRB-3F4 in SP64	This paper	N/A
WRB-3xFLAG in SP64	This paper	N/A
mEGFP-CAML L248K-P2A-mCherry in pcDNA5/FRT/TO	This paper	N/A
mEGFP-CAML L147K L248K L249K-P2A-mCherry in pcDNA5/FRT/TO	This paper	N/A
PrL signal seq-3xHA-CD4-GFP-P2A-RFP in pcDNA5/FRT/TO	This paper	N/A
PrL signal seq-3xHA-CAML tmd2-CD4-GFP-P2A-RFP in pcDNA5/FRT/TO	This paper	N/A
PrL signal seq-3xHA-GS linker-CD4-GFP-P2A-RFP in pcDNA5/FRT/TO	This paper	N/A
3xHA-CAML 1-195	This paper	N/A
3xHA-CAML 1-217	This paper	N/A
3xHA-CAML 1-227	This paper	N/A
3xHA-CAML 1-237	This paper	N/A
3xHA-CAML 1-247	This paper	N/A
3xHA-CAML 1-257	This paper	N/A
3xHA-CAML 1-267	This paper	N/A

REAGENT or RESOURCE	SOURCE	IDENTIFIER
3xHA-CAML 1-277	This paper	N/A
3xHA-CAML 1-287	This paper	N/A
3xHA-CAML 1-297	This paper	N/A
3xHA-CAML 1-304	This paper	N/A
3xFLAG-CAML M225C-3F4 in SP64	This paper	N/A
3xFLAG-CAML S250M-3F4 in SP64	This paper	N/A
3xFLAG-CAML C284M-3F4 in SP64	This paper	N/A
Software and Algorithms		
ImageJ	Schneider et al., 2012	<a href="https://imagej.nih.gov/ij/">https://imagej.nih.gov/ij/</a>
FlowJo	FlowJo	<a href="https://www.flowjo.com">https://www.flowjo.com</a>
Adobe Illustrator	Adobe	<a href="https://www.adobe.com/uk/creativecloud.html">https://www.adobe.com/uk/creativecloud.html</a>
Zeiss Zen	Zeiss	<a href="https://www.zeiss.com/microscopy/us/products/microscope-software/zen.html">https://www.zeiss.com/microscopy/us/products/microscope-software/zen.html</a>
Other		
Rabbit Reticulocyte Lysate Mix	Sharma et al., 2010	N/A
Canine rough microsomes	Walter and Blobel, 1983	N/A
TransIT-293 transfection reagent	Mirus	Cat. #MIR2705
DMEM, high glucose, GlutaMAX Supplement, pyruvate	Thermo Scientific	Cat. #10569010
RNAiMAX lipofectamine	Thermo Scientific	Cat. #13778150
Tetracycline-free Fetal Calf Serum (FCS)	BioSera	Cat. #FB-1001T/500